Fabrication and electrochemical performance of graphene–ZnO nanocomposites*

Li Zhen-Peng(李振鹏), Men Chuan-Ling(门传玲)†, Wang Wan(王 婉), and Cao Jun(曹 军)

School of Energy and Power Engineering, University of Shanghai for Science and Technology, Shanghai 200093, *China*

(Received 15 October 2013; revised manuscript received 25 November 2013; published online 18 March 2014)

Graphene–ZnO nanocomposites were synthesized successfully through a one-step solvothermal approach. The morphology, structure, and composition of the prepared nanocomposites were investigated by scanning electron microscopy (SEM), transmission electron microscope (TEM), laser micro Raman spectroscopy, and Fourier transform infra-red spectroscopy (FT-IR). The outcomes confirmed that this approach is comparatively steady, practicable, and operable compared with other reported methods. The electrochemical performance of the graphene-ZnO electrodes was analyzed through cyclic voltammetry, altering-current (AC) impedance, and chronopotentiometry tests. The graphene–ZnO electrodes exhibited an improved electrode performance with higher specific capacitance (115 $F\cdot g^{-1}$), higher electrochemical stability, and higher energy density than the graphene electrodes and most reported graphene–ZnO electrodes. Graphene–ZnO nanocomposites have a steady reversible charge/discharge behavior, which makes them promising candidates for electrochemical capacitors (ECs).

Keywords: graphene–ZnO nanocomposites, electrochemical performance, electrochemical capacitors

PACS: 72.80.Tm, 82.45.Rr, 82.47.Uv **DOI:** 10.1088/1674-1056/23/5/057205

1. Introduction

Electrochemical capacitors (ECs), which are also called supercapacitors, possess high energy and high power density, and have a long cycle life. As an ideal electrical energy storage device, ECs have drawn considerable attention. According to the charge storage mechanism, ECs are classified into electrochemical double layer capacitors (EDLCs) and pseudocapacitors (or redox supercapacitors). The former is based on activated carbons and its capacitance is proportional to the electrode surface area. In contrast, the latter uses transition metal oxides or electrical conducting polymers as electrode materials and they depend on fast Faradaic redox reactions.[1] However, both kinds of capacitors have obvious shortcomings: EDLCs possess high power density and long cycle life but low energy density while pseudocapacitors possess high energy density but poor cycle performance. In view of this, ECs based on composites are proposed because they possess a long cycle life, as well as offering high energy and high power density.

Among various carbon-based nanostructured materials, graphene is used as an electrode material for ECs due to its remarkable conductivity, excellent chemical stability, high mobility of charge carriers, suitable pore size distribution, and good capacitive performance, as well as its high surface area (2630 $g\cdot m^{-2}$).[2–9] Graphene is actually a single layer of carbon atoms that are tightly packed into a two-dimensional honeycomb sp^2 carbon lattice.[10] To improve the capacitive performance of graphene-based energy storage materials, they are usually doped with metal oxides, such as RuO_2, IrO_2, MnO_2, and NiO_x, because these metal oxides can contribute pseudocapacitance to the total capacitance in addition to the double layer capacitance provided by the carbon materials.[11–15] However, most metal oxides suffer from low abundance and high cost.[16] As an important wide band gap (3.37 eV) semiconductor, zinc oxide (ZnO) offers tremendous potential applications, especially in electronic and optical systems.[17–22] It is also a well-known active material with a high energy density of 650 $A\cdot g^{-1}$.[23] Therefore, many researchers have been prompted to synthesize graphene–ZnO nanocomposites and explore their properties.

Currently, there are few reports on the use of graphene–ZnO nanocomposites as electrode materials for ECs.[24–27] Lu *et al.* twice reported the use of graphene–ZnO nanocomposites for EC electrodes, which were fabricated using an ultrasonic spray pyrolysis method that exhibited specific capacitances of 11.3 $F\cdot g^{-1}$ and 61.7 $F\cdot g^{-1}$ in 1 M KCl solution.[28,29] Guo *et al.* fabricated a sandwiched-type of reduced GO–ZnO nanorods and reduced graphene oxide (GO) on a flexible PET substrate for EC applications, and a capacitance of 51.6 $F\cdot g^{-1}$ was obtained at a scan rate of 10 $mV\cdot s^{-1}$.[30] Using a microwave-assisted method, Ramadoss *et al.* synthesized graphene–ZnO nanocomposites that showed a capacitance of 109 $F\cdot g^{-1}$ at a scan rate of 5 $mV\cdot s^{-1}$ in a 1 M KCl solution.[31] Wang *et al.* successfully fabricated graphene–ZnO nanocomposites using glucose as the reducing agent, which exhibited

*Project supported by the National Project of University of Shanghai for Science and Technology, China (Grant No. 14XPM06) and the Natural Science Foundation of Shanghai, China (Grant No. 13ZR1428200).

†Corresponding author. E-mail: 2215752815@qq.com

© 2014 Chinese Physical Society and IOP Publishing Ltd

a specific capacitance of 62.2 $F \cdot g^{-1}$.[32] In addition, a hybrid structure of ZnO on a three dimensional (3D) graphene foam has been synthesized by chemical vapor deposition (CVD) under hydrothermal conditions, and the specific capacitance even reached 400 $F \cdot g^{-1}$.[33]

Generally speaking, high temperature, special equipment, and complicated conditions are essential in most above fabrication methods. Meanwhile, the solution methods include convenient and low cost approaches for the synthesis of ZnO nanocrystals, and the development of various graphene-based composites.[34,35] Unfortunately, due to the van der Waals interactions among graphene sheets in the reduction process, they are not steady and tend to agglomerate in the solution.[36,37]

In this paper, the graphene oxide is first prepared by the modified Hummers approach.[38,39] Next, we attempt to fabricate graphene–ZnO nanocomposites through a one-step solvothermal approach, making the *in-situ* growth ZnO particles decorate on the surfaces of graphene sheets randomly, we then investigate and discuss their properties.[40,41] The new strategy tends to be operated easily and it provides a novel improved electrochemical performance of graphene–ZnO nanocomposites used as the EC electrodes. The morphology, structure, and composition of the graphene–ZnO nanocomposites are investigated by scanning electron microscopy (SEM), transmission electron microscope (TEM), a laser micro Raman spectrometer, an X-ray diffractometer (XRD), and a Fourier transform infra-red spectrometer (FT-IR). Using a three-electrode system, the electrochemical performance of the graphene–ZnO nanocomposites is analyzed through cyclic voltammetry, alternating current (AC) impedance, and chronopotentiometry tests.

2. Experiment

2.1. Preparation of graphene oxide

Firstly, the graphene oxide was prepared successfully from expandable graphite powder by the modified Hummers approach. Briefly, expandable graphite powder (2 g) was added into a concentrated H_2SO_4 solution (40 mL) under ice-bath cooling and stirring for 2 h. Then, $KMnO_4$ (6 g) was slowly added into the solution under stirring and the temperature of reaction was kept lower than 20 °C. The mixture was then stirred at 35–40 °C for 30 min and at 65–80 °C for 45 min in succession. Deionized water (50 mL) was added to the obtained solution to dilute it and the mixture was heated at 90 °C for 30 min, leading to a dark brown solution. After additional stirring for 2 h, the dark brown solution was further diluted with distilled water (150 mL) and then H_2O_2 (10 mL, 30%) was added slowly at room temperature, the color of the mixture turned a brilliant yellow. After precipitation for 12 h, the upper supernatant was collected and centrifuged, where GO powder was obtained as the precipitates. To remove the metal ions existing in the GO powder, it was dissolved in an HCl solution (10%). Finally, the GO powder was further dissolved in deionized water (150 ml). The resulting precipitate was sonicated well in a probe type sonicator for nearly 1 h to obtain a uniform suspension of GO. After being centrifuged and dried at 60 °C in a hot air oven, GO was obtained as gray powder.

2.2. Synthesis of graphene–ZnO nanocomposites

The purified GO (50 mg) was dissolved in ethyleneglycol (20 mL) and sonicated for 30 min at room temperature to obtain a sufficient dispersion in the GO solution. Zinc acetate ($ZnC_4H_6O_4 \cdot 2H_2O$, 1 g) was added into ethylene glycol (30 mL). The prepared zinc acetate solution was then dissolved in the prepared GO solution with magnetic stirring. An NaOH solution was added into the mixture solution to adjust PH to 9 and it was stirred for 30 min ($Zn(OH)_2$ particles were formed and they decorated on GO). Then, hydrazine hydrate (0.03 ml) was added to reduce GO and the solution was placed in the reaction still at 160 °C for 24 h ($Zn(OH)_2$ particles resolved to ZnO particles and H_2O at 125 °C). The obtained composites were then centrifuged, washed by deionized water, and dried in a vacuum oven at 60 °C for 24 h, resulting in the formation of graphene–ZnO nanocomposites (Fig. 1).

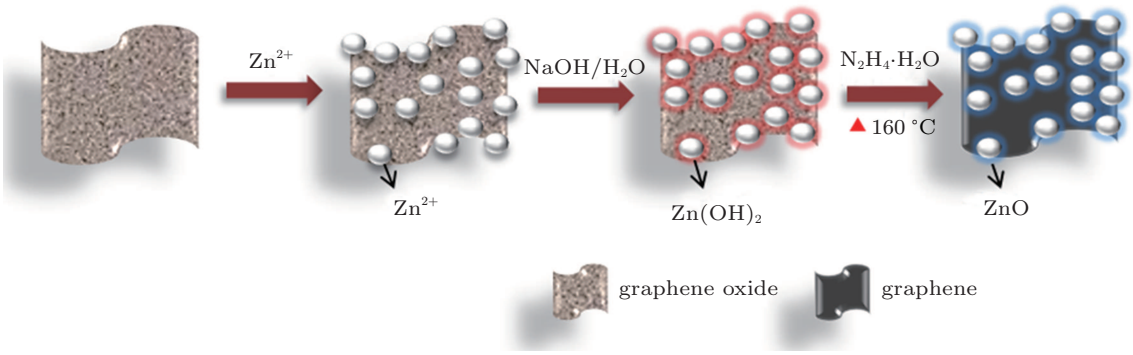


Fig. 1. (color online) Schematic fabrication of the growth process of the graphene–ZnO nanocomposites.

2.3. Morphology and compositional analysis

The morphology of the composites was investigated by SEM (Quanta FEG, FEI Co., Ltd.) and TEM (FEI Tecnai G2 F20 S-Twin). The phase composition was investigated by a Rigaku D-max-rB rotating positive pole X-Ray diffractomer with Cu $K\alpha$ radiation (at a scan rate of 8 °·min^{-1}, 10°–90°, 12 kW, sample interval of 0.2°), a Raman microscope (LabRam-1B, JY Co., Ltd.), and an FT-IR spectrometer (Nicolet Nexus 470, NICONET Co., Ltd.).

2.4. Electrochemistry tests

The obtained nanocomposites were mixed with acetylene black at a quantity rate of 85:15. The mixture was then pressured on the foam nickel to form electrodes. The electrochemistry tests were performed through the three-electrode system (counter electrodes and reference electrodes were made by platinum sheets and saturated calomel electrodes, respectively), using KOH (6 mol·L^{-1}) as the electrolyte. An electrochemical workstation (CHI660D, Shanghai Chenhua Co., Ltd.) was used to investigate the cyclic voltammetry, AC impedance, and chronopotentiometry.

3. Results and discussion

Figure 2 shows the XRD patterns of graphene–ZnO nanocomposites (GZO) and GO. As can be seen, the peak corresponding to the (001) crystalline plane of GO appears at around the scattering angle of 10.6° and is high.[42] The pattern of GZO shows that there are nine main peaks at $2\theta =$ 31.7°, 34.4°, 36.2°, 47.5°, 56.6°, 62.8°, 66.3°, 67.9°, 67.9°, corresponding to (100), (002), (101), (102), (110), (103), (200), (112), and (201) crystalline planes of ZnO, respectively. This result indicates the wurtzite structure of the ZnO particles on the graphene sheets. However, there are no typical peaks of GO or graphite (no crystal peak at around $2\theta = 26.5°$), indicating that the stratiform GO and graphite have been stripped from GZO. Because recent researches have shown that if the GO or graphite in the state of agglomeration is destroyed (such as stripped), its diffraction peaks become very weak and can even disappear.[43,44] The particle size of ZnO in graphene–ZnO nanocomposites can be estimated via the Scherrer equation by using the full widths at half-maximum of the peaks belonging to ZnO, and is calculated to be 12 nm.

Figure 3 shows the SEM and TEM images of the graphene–ZnO nanocomposites. As can be seen clearly from Figs. 3(a) and 3(b), the graphene sheets are randomly covered by densely packed ZnO particles due to the remaining oxygen functional groups. Due to the large specific surface area, the nanocomposites seem to be agglomerated, like a coral reef. The aggregation probably occurs during the drying process. Direct evidence of the formation of ZnO nanoparticles on the graphene sheets is given by TEM and HRTEM (Figs. 3(c) and 3(d)). It can be observed that the graphene sheets are decorated by the ZnO particles with an average size of 11–13 nm, which is consistent with the Scherrer equation analysis. The HRTEM image further shows that the surfaces of the graphene sheets are composed of crystalline ZnO.[45,46] The lattice spacing of planes is 0.28 nm, corresponding to the (100) crystal plane of ZnO, which is consistent with the d spacing reported in JCPDS (No. 36-1451).

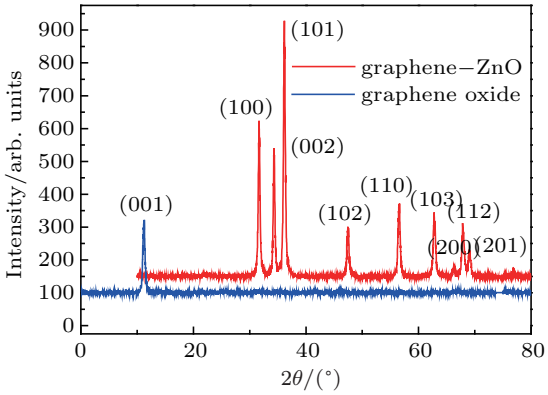


Fig. 2. (color online) XRD patterns of GZO and GO.

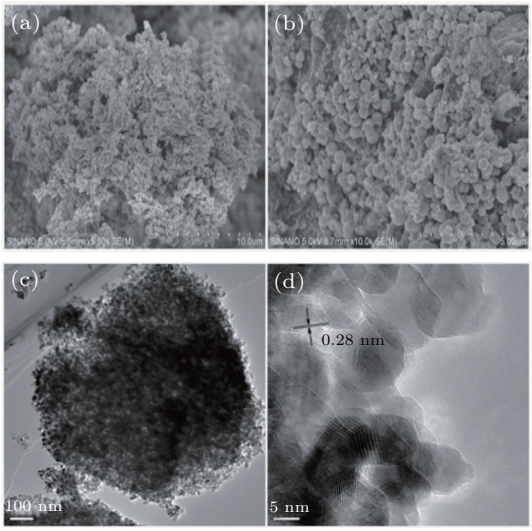


Fig. 3. (a) SEM, (b) SEM, (c) TEM, and (d) HRTEM images of graphene–ZnO nanocomposites.

The Raman spectrum is one of the best ways to characterize the bonding, ordering, and crystallite size in carbon materials. Figure 4 shows the Raman spectra of GZO and GO. As can be seen in Fig. 4, the spectrum of GO displays two absorption peaks at 1350 cm^{-1} (peak D) and 1590 cm^{-1} (peak G), corresponding to the breathing mode of κ-point phonons of A_{1g} symmetry and the E_{2g} phonon of the ordered C sp^2 atoms, respectively. Furthermore, peak D relates to the defect on the edge of the graphene and the amorphous structure.[47] The microstructure of GO is investigated by the Raman spectrum

mainly through the intensity ratio of peak D to peak G, which is related to the crystallite dimension (L_a) of the graphene samples, $I(D)/I(G) \propto 1/L_a$.[48] Compared with GO, $I(D)/I(G)$ of GZO is enhanced significantly, indicating that partial GO is reduced to graphene.[49–51] In addition, the scattering peaks of ZnO are weak due to the low annealing temperature, which leads to the insufficient crystallinity of ZnO and an unsatisfactory grain size.

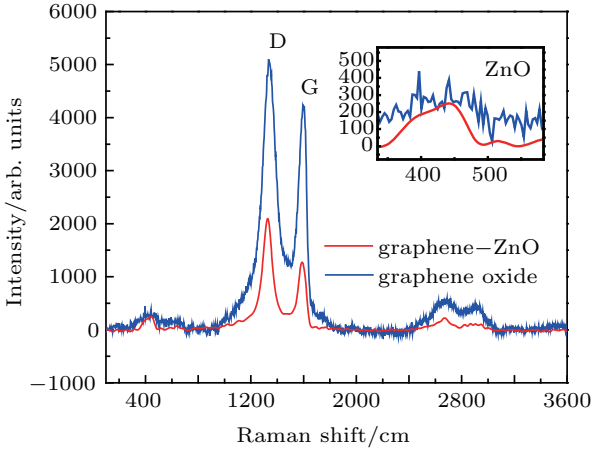


Fig. 4. (color online) Raman spectra of GZO and GO.

In order to accurately describe the structure of the graphene in GZO and its combination pattern with ZnO, Fig. 5 shows the FT-IR spectra of GZO and GO. The presence of different types of oxygen functionalities in GO is confirmed by the characteristic bands. In the high frequency area at 3391 cm^{-1}, the absorption peak corresponds to stretching of OH groups, yet in 2000–3100 cm^{-1}, the wide spectral peak is due to the water molecules absorbed by GO, indicating the strong moisture absorption ability of GO. In the intermediate zone, the absorption peak at 1615 cm^{-1} corresponds to the remaining sp^2 character of graphene; the absorption peak at 1728 cm^{-1} is assigned to C=O stretching of COOH groups on the edge of GO; the absorption peak at 1215 cm^{-1} corresponds to the C–O–C deformation vibration of the epoxy symmetrical ring on the surface of GO;[52,53] and the absorption peak at 1060 cm^{-1} is assigned to C–O stretching vibrations mixed with C–OH bending. As the FT-IR spectrum of GZO shows, the absorption peak at 1092 cm^{-1} is attributed to the C–OH and the characteristics of GO have completely disappeared. The absorption peak is at around 1386 cm^{-1} owing to the vibration of the graphene sheets, which indicates the reduction of GO to graphene. The absorption peak at 424 cm^{-1} corresponds to the stretching vibration of ZnO. Furthermore, the characteristic absorbance of CH_3COO– assigned to raw material zinc acetate is not found, confirming that the graphene–ZnO nanocomposites have been successfully synthesized.

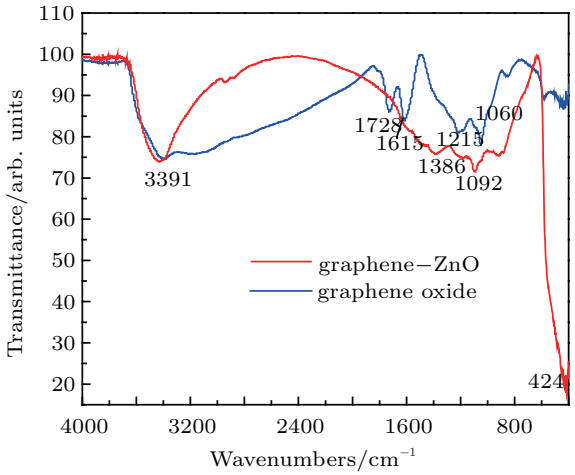


Fig. 5. (color online) FT-IR spectra of GZO and GO.

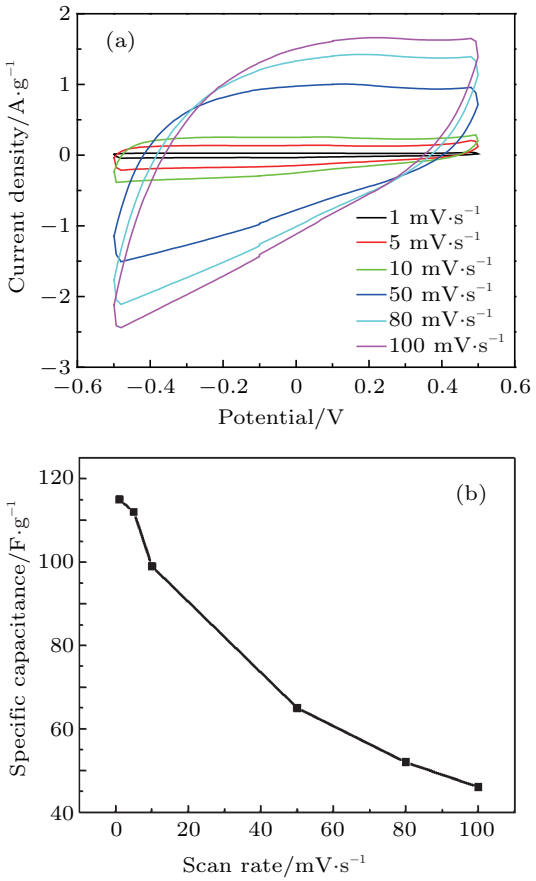


Fig. 6. (a) (color online) CV curves of GZO at different scan rates; (b) specific capacitances of GZO at different scan rates.

Figure 6(a) shows the cyclic voltammetric (CV) curves of GZO with different scan rates. It presents good symmetry at lower scan rate, indicating that the electrodes provide better reversibility under the condition of a small current discharge. All the CV curves are close to the rectangular shape, indicating an ideal capacitive property and an excellent reversibility of this electrode. The improved performance originates from the interaction of the pseudocapacitor and electric double layer capacitance. Figure 6(b) presents the multiple

performance curve resulted by cyclic voltammetry. At a scan rate of 1 mV·s^{-1}, the specific capacitance reaches 115 F·g^{-1}. With an increase of the scan rate, the specific capacitance decreases significantly. When the scan rate reaches 100 mV·s^{-1}, the electrochemical polarization becomes very serious, the specific capacitance drops to 46 F·g^{-1} and the specific capacitance retention rate is only 40%. This happens because the electrochemical and concentration polarizations become worse with the faster scan rate,leading to a decrease of the utilization rate of the electrode's active materials.

Figure 7 shows the Nyquist plots of GZO. In the high frequency range, the intersection of the curve with the x axis is the electrolyte resistance ($R_{\rm E}$), with a value of only 0.6 Ω. Actually a low internal resistance is important in an energy storage device because it can reduce unnecessary energy loss during the process of charge/discharge. It is measured that the GZO has a low charge transfer resistance (6.5 Ω) compared to that of graphene (9.8 Ω), indicating that the incorporation of ZnO improves the charge transfer performance of graphene electrodes. The straight line closed to 60° in the intermediate zone is related to the diffusive resistance (Warburg impedance) of the electrolyte into the interior of the electrode and the ion diffusion into the electrode surface. There is no vertical straight line in the low-frequency area, representing that the capacitor resulted not only from the electric double layer capacitor but also came from the pseudocapacitor.

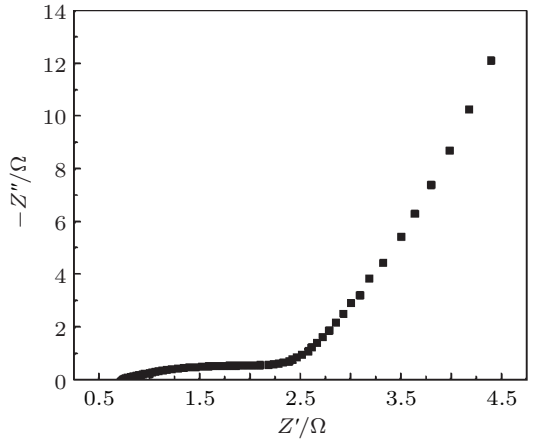


Fig. 7. Nyquist plots of GZO.

Figure 8(a) is the charge/discharge curve of GZO for the current density of 10 mA·g^{-1}. There are two decreasing voltage areas: from −0.2 V to 0 V and from −1 V to −0.2 V. The former with a short discharge process is controlled by the electric double layer capacitor. The discharge time of the latter is longer due to the pseudocapacitor produced by the electric double layer capacitor and ZnO. Figure 8(b) shows the corresponding multiple performance. The specific capacitance is 71 F·g^{-1} for the 10 mA·g^{-1} current density. As the current density increases, the specific capacitance decreases. With 1000 mA·g^{-1} current density, the specific capacitance is only 9 F·g^{-1} and the capacitance retention rate is 13%.

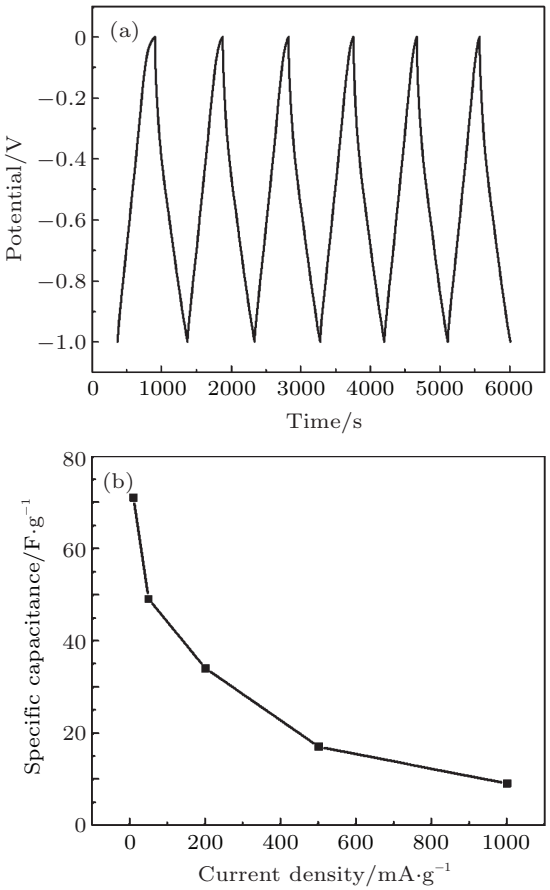


Fig. 8. (a) Charge/discharge curve of GZO for the current density of 10 mA·g^{-1} and (b) plots of current density versus specific capacitance of GZO.

4. Conclusion

In summary, graphene–ZnO nanocomposites have been successfully synthesized through a one-step solvothermal approach and their morphology, structure, composition, and electrochemical performance were investigated. Compared with other methods, with essential strict conditions and comparative uncontrollability of the processes, the one-step solvothermal approach is steady, practicable, and operable. The graphene–ZnO nanocomposites exhibited an improved electrode performance with higher specific capacitance, higher electrochemical stability, and higher energy density than the graphene electrodes. The graphene–ZnO nanocomposites achieved an excellent capacitance of 115 F·g^{-1} at a scan rate of 1 mV·s^{-1}. The improved supercapacitance of the graphene–ZnO nanocomposites compared with graphene is mainly due to the additional contribution from ZnO to the total capacitance, apart from the double layer capacitance. Tests also indicated that there is a serious concentration polarization at high scan rates. In brief, graphene–ZnO nanocomposites have great potential applications in ECs.

References

[1] Stephanie L, Shao Y Y, Zhou W, Li X L, Jie X, Zhang J G, Wang J, Liu J, Li J H and Cao G Z 2012 *Nano Energy* **1** 195
[2] Yang J S, Huang D H, Cao Q L, Li Q, Wang L Z and Wang F H 2013 *Chin. Phys. B* **22** 098101
[3] Guo S J and Dong S J 2011 *Chem. Soc. Rev.* **40** 2644
[4] Zhang X, Sun X, Chen Y, Zhang D and Ma Y 2012 *Mater. Lett.* **68** 336
[5] Lu M M, Yuan J, Wen B, Liu J, Cao W Q and Cao S 2013 *Chin. Phys. B* **22** 037701
[6] Novoselov K S, Geim A K, Morozov S V, Jiang D, Zhang, Dubonos S V, Grigorieva I V and Firsov A A 2004 *Science* **306** 666
[7] Wang J Y, Li Z Q, Fan G, Pan H H, Chen Z and Zhang D 2012 *Scripta Mater.* **66** 594
[8] Liu Y Z, Li Y F, Yang Y G, Wen Y F and Wang M Z 2013 *Scripta Mater.* **68** 301
[9] Li Y F, Liu Y Z, Shen W Z, Yang Y G, Wen Y F and Wang M Z 2011 *Mater. Lett.* **65** 2518
[10] Geim A K and Novoselov K S 2007 *Nat. Mater.* **6** 183
[11] Chen S, Zhu J, Wu X, Han Q and Wang X 2010 *ACS Nano* **4** 2822
[12] Lee B J, Sivakkumar S R, Ko J M, Kim J H, Seong M J and Dong Y K 2007 *J. Power Sources* **168** 546
[13] Shan Y and Gao L 2007 *Mater. Chem. Phys.* **103** 206
[14] Yan J, Fan Z J, Wei T, Qian W Z, Zhang M and Wei F 2010 *Carbon* **48** 3825
[15] Kyeong-Won P and Jong H J 2012 *J. Power Sources* **199** 379
[16] Zhang Y P, Li H B, Pan L K, Lu T and Sun Z 2009 *J. Electroanal. Chem.* **634** 68
[17] Zhang P Z, Li R S, Pan X J and Xie E Q 2013 *Chin. Phys. B* **22** 058106
[18] Wang Y, Li X, Wang N, Quan X and Chen Y 2008 *Sep. Purif. Technol.* **62** 727
[19] Tian C, Li W, Pan K, Zhang Q, Tian G, Zhou W and Fu H 2010 *J. Solid State Chem.* **183** 2720
[20] Kind H, Yan H, Messer B, Law M and Yang P 2002 *Adv. Mater.* **14** 158
[21] Huang M H, Mao S, Feick H, Yan H, Wu Y, Kind H, Weber E, Russo R and Yang P 2001 *Science* **292** 1897
[22] Wan Q, Li Q H, Chen Y J, Wang T H, He X L, Li J P and Lin C L 2004 *Appl. Phys. Lett.* **84** 3654
[23] Ito Y, Nyce M, Plivelich R, Klein M, Steingart D and Banerjee S 2011 *J. Power Sources* **196** 2340
[24] Zeng H D, Cao Y, Xie S F, Yang J H, Tang Z H, Wang X Y and Sun L Y 2013 *Nanoscale Res. Lett.* **8** 133
[25] Chen Y L, Hu Z A, Chang Y Q, Wang H W, Zhang Z Y, Yang Y Y and Wu H Y 2011 *J. Phys. Chem. C* **115** 2563
[26] Bai S and Shen X P 2012 *RSC Adv.* **2** 64
[27] Qu J, Luo C Q and Cong Q 2011 *Nano-Micro. Lett.* **3** 115
[28] Zhang Y, Li H, Pan L, Lu T and Sun Z 2009 *J. Electroanal. Chem.* **634** 68
[29] Lu T, Zhang Y, Li H, Pan L, Li Y and Sun Z 2010 *Electrochim. Acta* **55** 4170
[30] Guo G, Huang L, Chang Q, Ji L, Liu Y, Xie Y, Shi W and Jia N 2011 *Appl. Phys. Lett.* **99** 83111
[31] Ananthakumar R and Kim S J 2013 *Mater. Chem. Phy.* **140** 405
[32] Wang J, Gao Z, Li Z S, Wang B, Yan Y X, Liu Q, Mann T, Zhang M and Jiang Z H 2011 *J. Solid State Chem.* **184** 1421
[33] Dong X C, Cao Y F, Wang, J, Chan-Park M B, Wang L H, Huang W and Chen P 2012 *RSC Adv.* **2** 4364
[34] Zhu J W, Liu H B, Liu X H, Wang X, Yang X J and Lu L D 2009 *J. Wuhan Univ. Technol.* **24** 30
[35] Lambert T N, Chavez C A, Hernandez-Sanchez B, Lu P, Bell N S, Ambrosini A, Friedman T, Boyle T J, Wheeler D R and Huber D L 2009 *J. Phys. Chem. C* **113** 19812
[36] Li D, Müller M B, Gilje S, Kaner R B and Wallace G G 2008 *Nat. Nanotechnol.* **3** 101
[37] Lu T, Pan L K, Li H B, Zhu G, Lv T, Liu X J, Sun Z, Chen T and Daniel H C 2011 *J. Alloys Compd.* **509** 5488
[38] Hummers W S and Offeman R E 1958 *J. Am. Chem. Soc.* **80** 1339
[39] Krishnamoorthy K, Mohan R and Kim S J 2011 *Appl. Phys. Lett.* **98** 244101
[40] Liu Y Z, Li Y F, Yang Y G, Wen Y F and Wang M Z 2013 *Scripta Mater.* **68** 301
[41] Zou W B, Zhu J W, Sun Y X and Wang X 2011 *Mater. Chem. Phys.* **125** 617
[42] Li Q, Li Z, Chen M and Fang Y 2009 *Nano Lett.* **9** 2129
[43] Xu C, Wang X and Zhu J 2008 *J. Phys. Chem. C* **112** 19841
[44] Cai D and Song M 2007 *J. Mater. Chem.* **17** 3678
[45] Tian Y, Lu H B, Liao L, Li J C and Liu C 2009 *Solid State Commun.* **149** 456
[46] Feng L B, Liu A H, Liu M, Ma Y Y, Wei J and Man B Y 2010 *Mater. Charact.* **61** 128
[47] Obraztsov and Nat A N 2009 *Nat. Nanotechnol.* **4** 212
[48] Li X, Zhao W F and Chen G H 2008 *Mater. Rev.* **22** 48
[49] Stankovich S, Dikin D A, Piner R D, Kohlhaas K A, Kleinhammes A, Jia Y, Wu Y, Nguyen S T and Ruoff R S 2007 *Carbon* **45** 1558
[50] Park S, An J, Jung I, Piner R D, An S J, Li X, Velamakanni A and Ruoff R S 2009 *Nano Lett.* **9** 1593
[51] Wang H, Wang L, Qu C Q, Su Y D, Yu S S, Zheng W T and Liu Y C 2011 *J. Solid State Chem.* **184** 881
[52] Nethravathi C and Rajamathi M 2008 *Carbon* **46** 1994
[53] Matsuo Y, Miyabe T, Fukutsuka T and Sugie Y 2007 *Carbon* **45** 1005